

# Solid-State NMR Investigation of Drug-Excipient Interactions and Phase Behavior in Indomethacin-Eudragit E Amorphous Solid Dispersions

Joseph W. Lubach<sup>1</sup> · Jonathan Hau<sup>1</sup>

Received: 31 October 2017 / Accepted: 8 February 2018 / Published online: 20 February 2018  
© Springer Science+Business Media, LLC, part of Springer Nature 2018

## ABSTRACT

**Purpose** To investigate the nature of drug-excipient interactions between indomethacin (IMC) and methacrylate copolymer Eudragit® E (EE) in the amorphous state, and evaluate the effects on formulation and stability of these amorphous systems.

**Methods** Amorphous solid dispersions containing IMC and EE were spray dried with drug loadings from 20% to 90%. PXRD was used to confirm the amorphous nature of the dispersions, and DSC was used to measure glass transition temperatures ( $T_g$ ).  $^{13}\text{C}$  and  $^{15}\text{N}$  solid-state NMR was utilized to investigate changes in local structure and protonation state, while  $^1\text{H}$   $T_1$  and  $T_{1\rho}$  relaxation measurements were used to probe miscibility and phase behavior of the dispersions.

**Results**  $T_g$  values for IMC-EE solid dispersions showed significant positive deviations from predicted values in the drug loading range of 40–90%, indicating a relatively strong drug-excipient interaction.  $^{15}\text{N}$  solid-state NMR exhibited a change in protonation state of the EE basic amine, with two distinct populations for the EE amine at  $-360.7$  ppm (unprotonated) and  $-344.4$  ppm (protonated). Additionally,  $^1\text{H}$  relaxation measurements showed phase separation at high drug load, indicating an amorphous ionic complex and free IMC-rich phase. PXRD data showed all ASDs up to 90% drug load remained physically stable after 2 years.

**Conclusions**  $^{15}\text{N}$  solid-state NMR experiments show a change in protonation state of EE, indicating that an ionic complex indeed forms between IMC and EE in amorphous solid dispersions. Phase behavior was determined to exhibit

nanoscale phase separation at high drug load between the amorphous ionic complex and excess free IMC.

**KEY WORDS** amorphous · drug-excipient interactions · formulation · stability · solid-state NMR

## ABBREVIATIONS

ASD	Amorphous solid dispersion
CP	Cross polarization
DSC	Differential scanning calorimetry
EE	Eudragit® E
FTIR	Fourier transform infrared spectroscopy
HPMCAS	Hydroxypropyl methylcellulose acetate succinate
HPMCP	Hydroxypropyl methylcellulose phthalate
IMC	Indomethacin
MAS	Magic-angle spinning
NMR	Nuclear magnetic resonance spectroscopy
PSSA	Polystyrene sulfonic acid
PVP	Poly(vinylpyrrolidone)
PVPVA	Poly(vinylpyrrolidone-co-vinyl acetate)
PXRD	Powder X-ray diffraction
RF	Radiofrequency
TOSS	Total sideband suppression
UV	Ultraviolet spectroscopy
XPS	X-ray photoelectron spectroscopy

Guest Editors: Tony Zhou and Tonglei Li

✉ Joseph W. Lubach  
lubach.joseph@gene.com

<sup>1</sup> Small Molecule Pharmaceutical Sciences, Genentech, Inc.  
1 DNA Way, South San Francisco, California 94080, USA

## INTRODUCTION

Drug-excipient interactions have long been an area of interest for pharmaceutical scientists, yet to date many of these interactions are still poorly understood today (1–6). Formulations contain one or more active ingredients combined with what are typically viewed to be “inert” inactive ingredients.

However, these “inert” ingredients often contain reactive and/or ionizable functional groups, and freely exchangeable molecules. Generic excipient compatibility studies are conducted during early development, and excipients that are found to accelerate degradation are then excluded from formulation development wherever possible. Deeper understanding of the nature of these interactions at the molecular level is desired in order to be able to strategically formulate more stable and better performing drug products.

Drug-excipient interactions can initiate at the particle-particle surface interface in particulate systems, or throughout a particle in molecularly dispersed systems such as amorphous solid dispersions (ASDs) (7–22). For example, Ueda and colleagues noted an anti-plasticization effect when indomethacin (IMC) was formulated with poly(vinyl alcohol-co-acrylic acid-co-methyl methacrylate) (23). This was attributed to strong specific hydrophilic and hydrophobic interactions between the drug and polymer that imparted improved physical stability over other polymers. Yuan and coworkers were able to use  $^{13}\text{C}$  solid-state NMR to estimate the relative ratios of three different modes of hydrogen bonding in IMC-PVP and IMC-PVPVA amorphous dispersions (24). The three different modes manifested as three different NMR chemical shifts for the carboxylic acid carbon, and the ratios modulated depending on the drug loading. From these data the authors were also able to estimate the acid-acid dimerization enthalpy and entropy for amorphous indomethacin.

While often thought to have negative consequences, specific drug-excipient interactions can also have a positive influence on the stability and performance of drug products. In the present work we examine the interaction between IMC and EE. IMC is a poorly water-soluble weak acid with a  $\text{p}K_{\text{a}}$  of 4.5, which has been extensively studied in a variety of amorphous systems (24–37). EE is a methacrylate copolymer with weakly basic 2-dimethylaminoethyl ester side-chains, rendering it soluble at  $\text{pH} < 5$ . The IMC-EE interaction was previously noted by Chokshi and coworkers through inspection of the glass transition temperature ( $T_{\text{g}}$ ) as a function of drug load (38). The authors noted a marked positive deviation from expected (e.g. Gordon-Taylor predicted)  $T_{\text{g}}$  values at elevated drug loading, and attributed the anti-plasticization effect to an intermolecular interaction between IMC and EE. Due to the acidic nature of IMC and basic nature of the polymer, a specific ionic interaction has been hypothesized as the molecular reason for the observed anti-plasticization effect. FTIR data were acquired, but no specific drug-polymer interaction was clearly evident in the data. However, it should be noted that this was not the focus of their study. In Sarode *et al.*, the investigators took a closer look at this specific interaction using FTIR, and concluded that the interaction between IMC and EE was improved upon storage of hot melt extrudates at elevated temperature and humidity (39). The authors correlated their FTIR data with results reported earlier by Kojima *et al.*

for a similar ionic interaction between mefenamic acid and EE (40). Liu and coworkers also reported on the IMC:EE interaction and drug-polymer miscibility using FTIR in addition to rheological measurements (41).

Ionic interactions in amorphous solid dispersions have been an area of interest in recent literature, and show promise as a platform for long-term stability of amorphous dispersions. Weuts and colleagues reported on ionic interactions in ASDs based on the acidic polymer poly(acrylic acid) (42). Formulations with three basic drugs all showed higher than expected  $T_{\text{g}}$  values, inhibition of crystallization, and faster dissolution rates. The ionic interaction was inferred from the carbonyl vibrational modes in the FTIR data. Song *et al.* showed that a specific acid-base drug-polymer interaction helped stabilize lapatinib-HPMCP dispersions, but not in dispersions with HPMCAS (43). Solid-state NMR proved to be very powerful in identifying these interactions. Subsequent studies by Song and coworkers verified the presence of specific acid-base interactions in PSSA based amorphous dispersions using UV, FTIR, XPS, and solid-state NMR, and in lumefantrine dispersions with five polymers using XPS (44,45).

In the present work we examine the potential ionic interaction between IMC and EE using solid-state NMR to directly ascertain the nature of the specific interaction. Unlike other spectroscopies such as FTIR, solid-state NMR has the power to selectively look at the specific nuclei involved in a drug-excipient interaction to remove ambiguity from the data interpretation. Using  $^1\text{H}$  relaxation measurements we also investigated the miscibility of IMC and EE and make inferences based on the mobility observed in the series of ASDs at differing drug loads. Long-term stability data using PXRD also show exquisite physical stability of the ASDs at all drug loadings up to 90% IMC ( $w/w$ ), indicating that truly ionic interactions in ASDs offer the potential for long term crystallization inhibition using only small amounts of polymer. This can potentially eliminate the tablet size and number burden often associated with high dose amorphous dispersion formulations that are formulated at low drug load due to crystallization propensity of the active ingredient. The data presented below focuses on the drug:excipient interactions and phase behavior of freshly prepared spray dried amorphous solid dispersions. We show long-term stability results using PXRD merely to demonstrate the exceptional physical stability that high drug load dispersions featuring ionic interactions can possess. We fully expect that water has a significant impact on phase behavior of amorphous dispersions, and that changes may occur on stability when disordered systems are exposed to moisture. This of course warrants further study and is another area where we feel that solid-state NMR spectroscopy can have an impact in pharmaceutical research.

## MATERIALS AND METHODS

### Materials

Crystalline indomethacin free acid (IMC) was purchased from MP Biomedicals, LLC (Solon, OH) and recrystallized from methyl isobutyl ketone as the  $\gamma$  polymorph. Eudragit® E PO (EE) was received as a gift from Evonik (Evonik Industries AG, Essen, Germany). Chemically, EE is poly(butyl methacrylate-co-(2-dimethylaminoethyl) methacrylate-co-methyl methacrylate) with a 1:2:1 subunit ratio.

### Spray Drying

Binary amorphous solid dispersions containing 20, 30, 40, 50, 60, 70, 80, and 90% IMC (*w/w*) in EE were spray dried using a ProCepT 4M8-S lab scale spray dryer (ProCepT NV, Zelzate, Belgium). Additionally, neat IMC and EE were also spray dried for reference data on the pure amorphous materials. The feed solutions were prepared at 10% solids loading in acetone (Thermo Fisher Scientific, Waltham, MA), and fed at 2 mL/min to a 1.0 mm spray nozzle. The inlet temperature was 80°C, outlet temperature was 38–40°C, air speed was 0.5 m<sup>3</sup>/min, and the cyclone pressure drop was ~26 mbar.

### p*K*<sub>a</sub> Calculation

Acid dissociation constants for EE subunits and oligomers were calculated using MoKa 2.6 (Molecular Discovery Ltd., Borehamwood, United Kingdom) and a custom semi-empirical p*K*<sub>a</sub> calculation model.

### Differential Scanning Calorimetry

DSC analysis was conducted using a TA Instruments Q2000 (New Castle, DE). A sample size of approximately 5 mg was weighed into a standard aluminum pan, covered with an aluminum lid but uncrimped. The samples were heated at 10°C/min from ambient temperature to 110°C under dry nitrogen at 50 mL/min. The samples were then cooled to 0°C at 20°C/min before being heated again to 180°C at 10°C/min under dry nitrogen at 50 mL/min.

### Density

Density measurements were made using a Micromeritics AccuPyc II 1340 helium pycnometer (Micromeritics Instrument Corp., Norcross, GA). ~1 g of powder was loaded into the measurement cell and 10 cycles were performed to give the average density. Standard deviations ranged from 0.0003–0.0082 g/cm<sup>3</sup>, and we report to the nearest 0.01 g/cm<sup>3</sup> here. The equilibration rate was 0.005 psig/min, and all data were acquired at 295 K.

### Powder X-ray Diffraction

Samples were analyzed using a Rigaku MiniFlex II powder X-ray diffractometer (Rigaku Americas Corp., The Woodlands, TX). The radiation used was CuK $\alpha$  with a tube voltage and current of 30 kV and 15 mA. Data were collected at ambient temperature from 2.0 to 40.0° 2 $\theta$  using a step size of 0.020°. A zero background silicon sample holder was used and the stage was rotated at 60 rpm. Soller slits employed on the incident and diffracted beam were 5°. The system was equipped with a variable divergence slit, 1.25° anti-scatter slit, 0.3 mm receiving slit, and a graphite monochromator. A scan speed of 2°/min was used. After initial analysis, samples were stored at 25°C/60% RH and analyzed for physical stability at 6 and 24 months of storage.

### Solid-State NMR Spectroscopy

All solid-state NMR data were acquired using a Bruker Avance III HD spectrometer with a 500 MHz Ascend standard bore magnet (Bruker BioSpin Corp., Billerica, MA). For each sample, ~80 mg of powder was packed into a 4 mm zirconia rotor and capped with a Kel-F drive tip. A double resonance MAS probe equipped with a 4 mm spinning module was used for all data collection, tuned to 500.13 MHz for <sup>1</sup>H, 125.77 MHz for <sup>13</sup>C experiments, and 50.69 MHz for <sup>15</sup>N experiments. <sup>13</sup>C-detected experiments utilized ramped cross polarization (CP) (46–48) with a 70–100% RF power ramp on the <sup>1</sup>H channel, 5 $\pi$  TOSS with a 243-step phase cycle (49,50), and high-power SPINAL64 (51) <sup>1</sup>H decoupling with an RF field strength of 86 kHz. <sup>15</sup>N-detected experiments employed ramped CP without TOSS. <sup>13</sup>C spectra were acquired using a 2 ms CP contact time, 2–4 s recycle delays, and 12 kHz MAS. <sup>15</sup>N spectra used a 2 ms CP contact time, 2–4 s recycle delays, and 8 kHz MAS. <sup>1</sup>H 90° pulses were 2.9  $\mu$ s for all experiments and TOSS used <sup>13</sup>C 180° pulses of 7.2  $\mu$ s. A total of 972 scans were collected for each <sup>13</sup>C spectrum and 70,000–100,000 scans were collected for each <sup>15</sup>N spectrum. The <sup>15</sup>N dipolar dephasing experiment utilized an interrupted decoupling period of 200  $\mu$ s, MAS rate of 4 kHz, and 41,472 scans were collected. <sup>1</sup>H relaxation experiments were <sup>13</sup>C-detected and utilized a 2 ms CP contact time, 8 kHz MAS, saturation recovery  $\tau$  delays of 0.005–20 s for *T*<sub>1</sub> measurements, and <sup>1</sup>H spin-lock pulses at 86 kHz ranged from 0.005–50 ms for *T*<sub>1 $\rho$</sub>  measurements. IMC carbon peaks in the range of 143–124 ppm were integrated to calculate IMC-specific relaxation times, and EE peaks in the range of 49–42 ppm were integrated to obtain EE-specific relaxation times. All data were recorded at 298 K. <sup>13</sup>C spectra were referenced to tetramethylsilane by using the methyl peak of 3-methylglutaric acid (MGA) at 18.84 ppm (52). <sup>15</sup>N spectra were referenced to nitromethane using the amino peak of glycine at –347.58 ppm (53). NMR data were processed using

Bruker TopSpin™ 3.2 software, and all  $^1\text{H}$  relaxation data were fitted using KaleidaGraph 4.1 software (Synergy Software, Reading, PA).

## RESULTS AND DISCUSSION

The chemical structures of IMC and EE are shown in Fig. 1. IMC is a carboxylic acid with a  $\text{p}K_a$  of 4.5, while EE is a methacrylate copolymer containing basic 2-dimethylaminoethyl ester side-chains with estimated  $\text{p}K_a$  ranging from 7.7–9.0. Conjugate acid dissociation constants for EE were calculated on various monomers and oligomers to gain a picture of the overall basicity of tertiary amine side-chain units in the polymer. This  $\Delta\text{p}K_a$  of 3.2–4.5 satisfies the widely used rule-of-thumb regarding  $\text{p}K_a$  differences ( $\Delta\text{p}K_a > 2$ ) between acids and bases for salt formation, and should be large enough to allow for proton transfer from the IMC acid to the EE amine group. This would serve to form an amorphous drug-polymer ionic complex at stoichiometries up until all of the basic polymer side-chain units are occupied by IMC. However, it should be noted that most dissociation constants referenced, measured, or calculated on pharmaceutical systems refer to values in aqueous solution. While obviously very useful, this does not necessarily reflect what the protonation state will be in an isolated solid, necessitating the use of solid-state characterization techniques to assess protonation state as it exists in the solid material of interest.

With a molecular weight of 357.79 g/mol, IMC contains 2.795 mmol of  $-\text{COOH}$  groups per gram of material. EE has an average molecular weight of  $\sim 47,000$  g/mol, but an oligomer containing a 1:2:1 ratio of butyl methacrylate, 2-dimethylaminoethyl methacrylate, and methyl methacrylate has a molecular weight of 556.74 g/mol. It follows that EE contains approximately 3.592 mmol of amino groups per gram of material. From this we calculate the stoichiometry of acidic to basic moieties in the drug-polymer dispersions. The molar ratios are shown in Table I for all drug-polymer

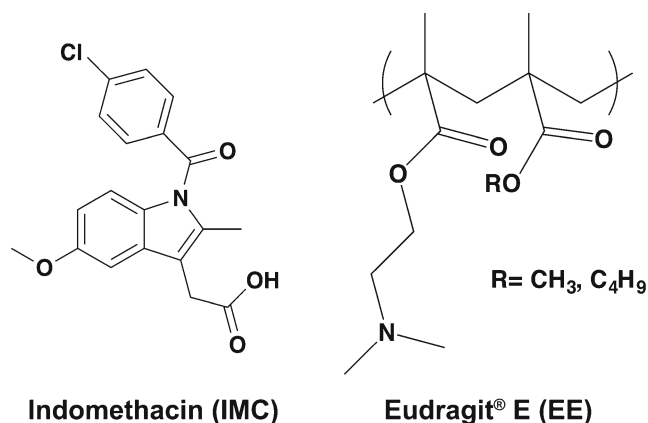


**Fig. 1** Chemical structures of indomethacin (IMC) and Eudragit® E (EE). The subunit ratio for EE polymer is 1:2:1 butyl methacrylate:2-dimethylaminoethyl methacrylate:methyl methacrylate.

**Table I** Molar Ratio of IMC  $-\text{COOH}$  Functional Groups to EE  $-\text{N}(\text{CH}_3)_2$  Functional Groups as a Function of Weight Percentage

IMC:EE Weight %	Molar Ratio ( $-\text{COOH}/\text{N}(\text{CH}_3)_2$ )
20:80	0.195
30:70	0.333
40:60	0.519
50:50	0.778
56.24:43.76 <sup>a</sup>	1.000
60:40	1.167
70:30	1.815
80:20	3.112
90:10	7.002

<sup>a</sup>Theoretical weight ratio to achieve a 1:1 molar ratio of acid-base functional groups

compositions prepared in this study. Additionally, the theoretical composition of 1:1 (mol/mol) IMC  $-\text{COOH}$  to EE  $-\text{N}(\text{CH}_3)_2$  is also shown with a drug-polymer composition of 56.24% IMC to 43.76% EE. In theory and in the absence of steric interference, above this drug-polymer ratio all EE amino side-chains should be protonated and occupied by an ionized IMC molecule. Thus, at 60, 70, 80, and 90% IMC, all amino groups in EE should be protonated and ionically bonded to an IMC carboxylate group.

## Thermal Analysis & Density

Pharmaceutical scientists often refer to the “ $T_g$  minus 50” rule of thumb, which suggests that an ASD should be stored at least 50 K below its glass transition temperature to maintain physical stability (54). This rule is primarily based on reducing molecular mobility in the glass to sufficiently slow or inhibit the crystallization propensity of the API, and thus provide adequate shelf-life of the drug product. In the present example, IMC has a  $T_g$  of 46°C, and EE has a  $T_g$  of 49°C (Fig. 2, Table II), both relatively low as neat materials. With ideal mixing in the absence of any intermolecular interactions, one could reasonably expect to obtain binary solid dispersions of the two materials with  $T_g$  values in the range of 46–49°C. Applying the  $T_g$ -50 rule would then require a highly undesirable storage requirement below 0°C. Plasticization with sorbed water molecules would further reduce the  $T_g$  and recommended storage temperature. Essentially this would likely preclude development of this amorphous system and a polymer with higher  $T_g$  would be selected.

However, an anti-plasticization effect was first observed by Chokshi and coworkers upon formulating IMC-EE ASDs at elevated drug loading (38). We desired to study this further and prepared ASDs in 10% ( $w/w$ ) intervals from 20 to 90% IMC. Using DSC we confirmed the anti-plasticization effect, as shown in Fig. 2. At 70% IMC, the  $T_g$  curve peaks out at

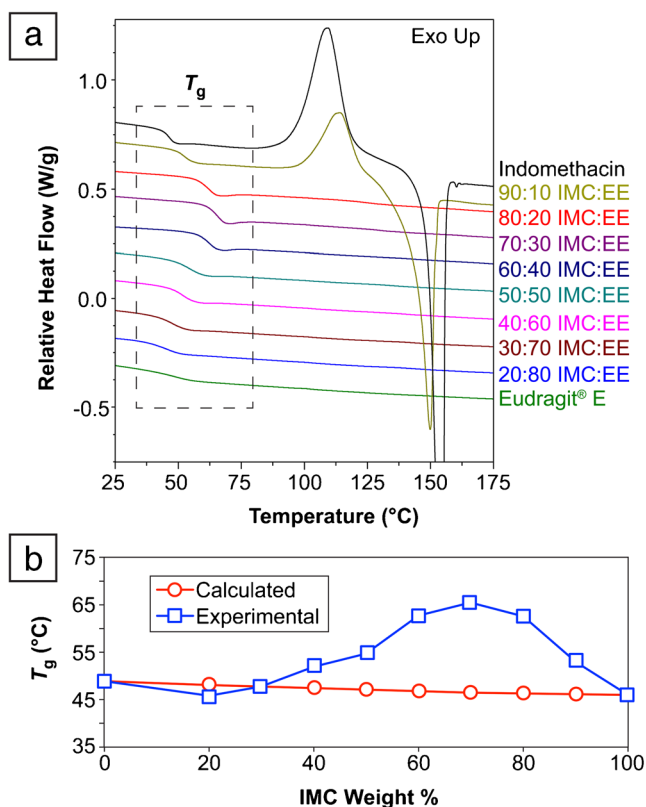


**Fig. 2** (a) DSC thermograms of amorphous IMC, EE, and amorphous solid dispersions containing both materials with compositions of 20–90% (w/w) IMC. Glass transitions ( $T_g$ ) are highlighted in the boxed region. (b)  $T_g$  of IMC-EE solid dispersions as a function of IMC weight fraction, compared to values calculated using the Couchman-Karasz convention.

65.5°C, which is nearly 20° above the expected value calculated using the Couchman-Karasz equation (55,56). From a mobility perspective alone, this has a huge impact on potential storage requirements and physical stability. The high drug loads of 60% and 80% IMC also offer a ~16° increase in  $T_g$  relative to calculated values. Furthermore, the heat capacity change ( $\Delta C_p$ ) also has a maximum at 70% IMC, and follows a similar trend as  $T_g$  throughout the range of dispersion

**Table II** Differential Scanning Calorimetry Data for Amorphous IMC:EE Systems Containing 0–100% (w/w) IMC, with Associated Densities

IMC:EE Weight %	$T_g$ (°C)	$\Delta C_p$ (J/g*K)	Density (g/cm <sup>3</sup> )
0:100	48.9	0.27	1.14
20:80	45.8	0.34	1.19
30:70	47.7	0.38	1.22
40:60	51.9	0.40	1.24
50:50	54.7	0.42	1.28
60:40	62.7	0.43	1.29
70:30	65.5	0.46	1.31
80:20	62.5	0.42	1.33
90:10	52.8	0.39	1.37
100:0	45.9	0.37	1.42

composition as shown in Table II. These high drug loads (60–80%) were once considered unattainable for amorphous dispersions, and have relegated many high dose amorphous drugs to large tablets and high doses of polymeric excipients. Interestingly, density varied linearly as a function of % IMC (Table II) and did not offer further insight into the nature of these systems. The observed anti-plasticization effects are a strong indicator of a specific, possibly ionic drug-polymer interaction, and warrant further study to confirm the nature of the interaction. Taking advantage of interactions like this may offer an easy path to stable high drug load amorphous formulations, reducing tablet size, excipient doses, and overall pill burden. For this reason, solid-state NMR studies were undertaken in attempt to provide nucleus-specific spectroscopic information on the interaction and are presented below, including <sup>13</sup>C and <sup>15</sup>N spectra as well as <sup>1</sup>H relaxation data.

### <sup>13</sup>C Solid-State NMR Spectroscopy

Solid-state NMR data offer a wealth of structural and dynamic information, even for disordered materials such as ASDs. <sup>13</sup>C spectra were first acquired to ascertain potential differences in the IMC –COOH peak(s) since this was suspected to undergo proton transfer to the polymer (Fig. 3). There are some other minor differences in the spectra, but the most interesting region lies from 170 to 180 ppm, where the carbonyl carbons resonate. It has already been reported that IMC carbonyl chemical shifts have multiple potential H-bonding motifs that all

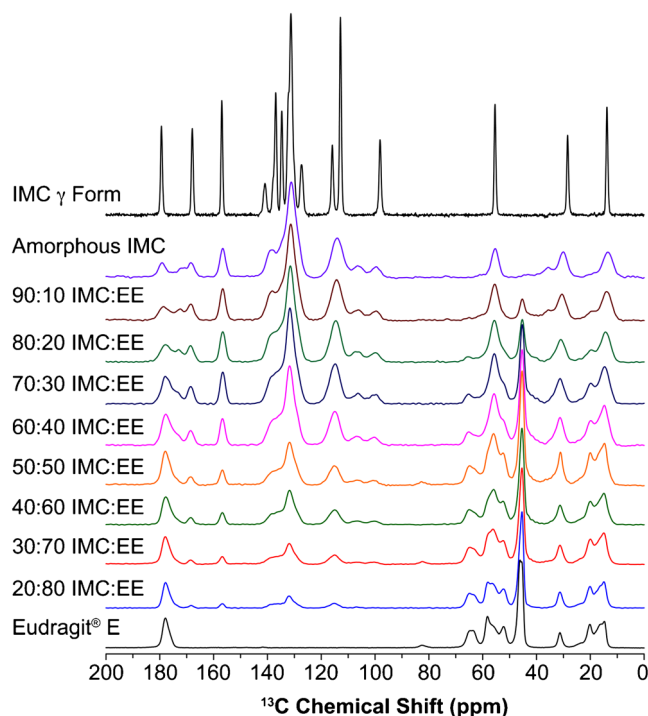


**Fig. 3** <sup>13</sup>C solid-state NMR spectra of EE, ASD samples of 20–90% IMC in EE, neat amorphous IMC, and crystalline IMC,  $\gamma$  form.

resonate at slightly different chemical shifts, resulting in multiple peaks for a single carbonyl nucleus in amorphous IMC (24). In crystalline  $\gamma$  IMC the leftmost peak at 179.2 ppm represents the carboxylic acid carbon, which forms a H-bonded cyclic dimer in this crystal form. The next peak to the right at 167.6 ppm is due to the amide carbonyl, which is not involved in H-bonding. In neat amorphous IMC it is evident that more than two peaks are present in this region, a clear indication of multiple different environments for the carbonyl carbons. The aforementioned work by Yuan and Munson definitively assigned the different  $-\text{COOH}$  resonances at 179.3 ppm to H-bonded cyclic dimers, 176.3 ppm an acid-acid H-bonded chain, acid H-bonded to amide at 172.4 ppm, and 170.4 ppm is free  $-\text{COOH}$  (24).

While these environments all appear to be present in our neat amorphous IMC, there are significant changes in this region of the spectrum across the range of drug loading as is evident in Fig. 3. Unfortunately the ester carbonyl peak of EE overlaps with much of the region of interest and restricts detailed interpretation of the different carboxylic acid states. There is a clear loss of the peaks at 172–176 ppm at drug loads below 50%, indicating loss of the acid-acid chain and acid-amide H-bonding modes. This would of course be the case if the IMC carboxylate carbon is exclusively involved in an ionic bond with EE amine groups. At higher drug loads of 60% and more, we observe a peak at  $\sim 173$  ppm which drifts more upfield as drug load increases to 90%. Since all ionic bonding possibilities are exhausted at  $\geq 60\%$  drug load, excess IMC carboxylic acid groups are free to H-bond with other acid and amide carbonyls of IMC or ester carbonyls in EE, which likely constitutes this series of peaks. We presume that the carboxylate chemical shift is similar to the acid-acid cyclic dimer, and thus is completely overlapped by the EE ester carbonyls. For this reason we pursued  $^{15}\text{N}$  solid-state NMR to further investigate the protonation state of amine groups in EE.

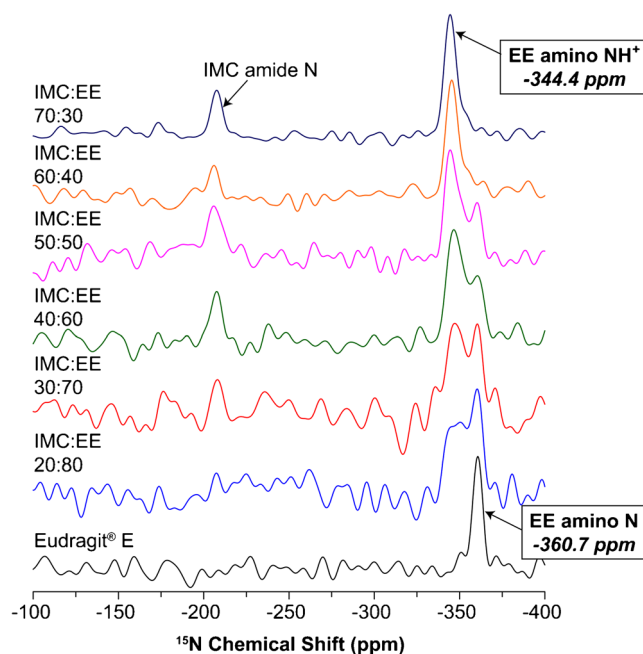
### $^{15}\text{N}$ Solid-State NMR Spectroscopy

While  $^{15}\text{N}$  is an extremely useful spin- $1/2$  nucleus with a wide chemical shift range, it suffers heavily from sensitivity issues due to its low magnetogyric ratio and natural abundance of only 0.37%. This makes acquisition of  $^{15}\text{N}$  NMR spectra at natural abundance challenging and time consuming, but feasible in reasonable amounts of time (e.g.  $<24$  h) for pure crystalline materials with sharp lines and relatively fast  $T_1$  relaxation times. For amorphous materials, all the signal intensity for a single nitrogen nucleus is spread out in a very broad, Gaussian peak, further reducing the sensitivity of nitrogen NMR. Amorphous materials often give peaks 5–10 $\times$  broader than their crystalline counterparts. Amorphous formulations such as ASDs further reduce sensitivity by diluting the nuclei of interest with other ingredients. In this case, the nitrogen-

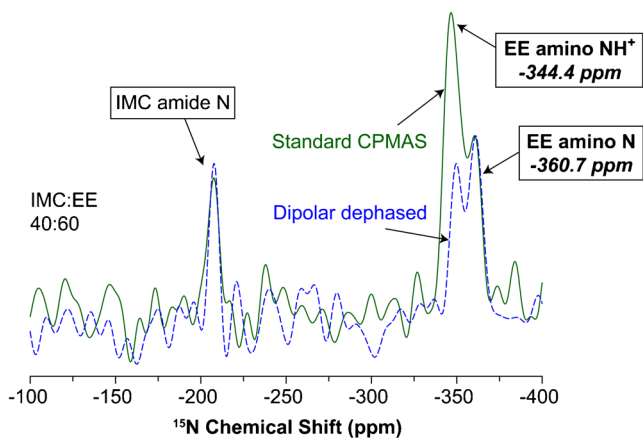
containing ingredient of interest is the polymeric excipient, specifically the EE 2-dimethylaminoethyl side-chain nitrogen nuclei. Due to the broad peaks and dilution by formulation, the spectra shown in Fig. 4 each took on the order of 4–5 days to acquire interpretable signal. However, the data demonstrate the value of  $^{15}\text{N}$  data in studying drug-excipient interactions where nitrogen atoms are involved.

Figure 4 shows the  $^{15}\text{N}$  solid-state NMR spectra for EE and ASDs containing 20–70% IMC. Neat EE gives a single peak for its neutral tertiary amine at  $-360.7$  ppm. Moving up the figure to 20% IMC, another population of this nitrogen is clearly evident. Increasing drug load leads to further increase in this population at  $-344.4$  ppm. At 70% IMC, there is once again a single amino peak, but at  $-344.4$  ppm is shifted 16.3 ppm downfield from the neutral polymer. For a tertiary amine, this large chemical shift change can only be due to protonation of the basic nitrogen. The data correlate well with the molar ratio calculations from Table I, which showed that above 56.24% IMC there should be enough IMC present to protonate all of the basic EE side-chains. In the  $^{15}\text{N}$  spectra of 60% and 70% IMC it is evident that essentially all of the EE amine groups have shifted to the protonated state and have formed ionic bonds with IMC. At 50% IMC and below, there are still excess unprotonated EE amine groups, as shown by the residual peak at  $-360.7$  ppm. This gives direct, specific spectroscopic evidence of amorphous ionic complex formation in the IMC-EE system.

To further verify that the chemical shift change is indeed due to protonation, a dipolar dephasing experiment was



**Fig. 4**  $^{15}\text{N}$  solid-state NMR spectra of Eudragit® E (EE) and ASD samples of 20–70% indomethacin (IMC) and EE.



**Fig. 5**  $^{15}\text{N}$  solid-state NMR spectra of 40:60 (w/w) indomethacin (IMC):Eudragit® E (EE) amorphous solid dispersion. The green (solid line) spectrum is the standard CPMAS spectrum, and the blue (dashed line) spectrum was acquired using a dipolar dephasing delay of 200  $\mu\text{s}$ .

attempted on the 40% IMC samples. The dipolar dephasing experiment turns off proton decoupling for a short period of time before signal acquisition. Nuclei exhibiting strong dipolar coupling to protons will rapidly dephase (i.e. lose signal intensity) during this period of interrupted decoupling. In  $^{13}\text{C}$  NMR, the experiment is routinely used to distinguish CH and  $\text{CH}_2$  carbons from quaternary and methyl carbons. Methyl carbons do not dephase rapidly due to the self-decoupling rotation of the protons about the C3 axis of the methyl group. For  $^{15}\text{N}$  NMR, dephasing times generally need to be longer, but the outcome of the experiment is analogous in that protonated nitrogen nuclei will lose signal (dephase) during the interrupted decoupling period. Figure 5 shows the results of a dipolar phasing experiment on the 40:60 IMC:EE sample, overlaid with the standard CPMAS spectrum, which clearly demonstrated two strong nitrogen populations at  $-344.4$  ppm and  $-360.7$  ppm. The overlay is scaled such that the IMC amide nitrogen and unprotonated EE amino nitrogen have the same intensity in both spectra, since these assignments are known to not have covalently attached

protons. In the dipolar dephased spectrum in Fig. 5 it is clear that the resonance at  $-344.4$  ppm has significantly decreased in intensity using a dephasing period of 200  $\mu\text{s}$ . This can only happen if the nitrogen nucleus is strongly coupled to a proton, which is governed by proximity (dipolar coupling  $\propto 1/r^3$ ). In a rigid crystal, covalently attached protons can dephase the signal to zero with a properly optimized dephasing time. The mobility and dynamics in an amorphous system can partially average the dipolar coupling and thus preclude full dephasing of the NH signal. Additionally, the sheer length of the experiment time required inhibited full optimization of the dephasing time. With these caveats noted, the only way for this nitrogen to dephase to this extent is due to close proximity to a covalently bound proton.

### Solid-State NMR $^1\text{H}$ Relaxation

Proton relaxation measurements have been in numerous reports used to probe drug-polymer miscibility in ASDs, and can assess phase separation much more selectively and at smaller domain sizes than classical DSC measurements (57–60). Here we applied  $^1\text{H}$   $T_1$  (spin-lattice relaxation time) and  $^1\text{H}$   $T_{1\rho}$  (spin-lattice relaxation in the rotating frame) measurements to look at IMC-EE phase miscibility, as it was especially intriguing given the fact that multiple phases may be present due to the formation of an amorphous ionically bonded complex not present in the neat starting materials. In general,  $^1\text{H}$   $T_1$  probes MHz-order motions and miscibility down to domain sizes of  $\sim 20$ – $50$  nm, and  $^1\text{H}$   $T_{1\rho}$  probes kHz-order motions and phase miscibility on the order of  $\sim 2$ – $5$  nm domain sizes (58). Using  $^{13}\text{C}$ -detected cross polarization experiments (magnetization transfer from  $^1\text{H}$  to  $^{13}\text{C}$ ), we can separate out resonances from each ASD component in the carbon spectrum, and calculate relaxation times for each individual component in the dispersion.  $^1\text{H}$  spin diffusion through the dipolar coupling network serves to average all the  $^1\text{H}$  relaxation rates in a given domain to a uniform value. If the relaxation times are similar (generally within 10%) for each

**Fig. 6**  $^1\text{H}$   $T_1$  and  $T_{1\rho}$  relaxation times for IMC-EE amorphous solid dispersions. The blue (IMC, circles) and red (EE, squares) curves show  $T_1$  values measured for each component in dispersions at each respective composition. The green (IMC, triangles) and purple (EE, diamonds) curves show  $T_{1\rho}$  values measured for each component in dispersions at each respective composition.

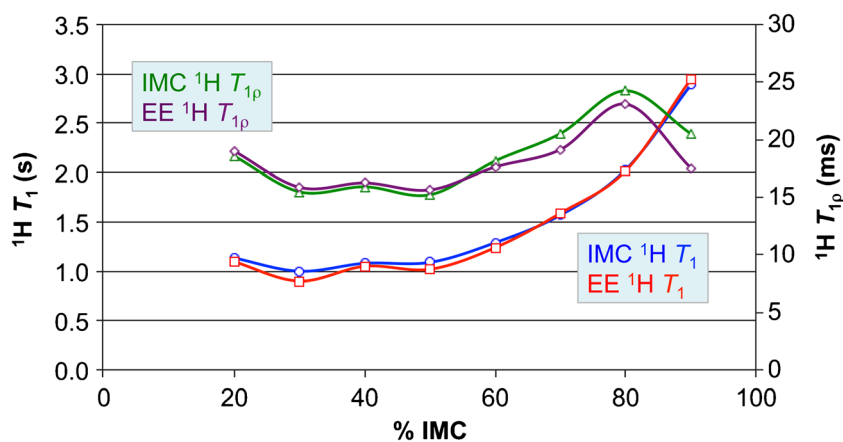


**Table III**  $^1\text{H}$  Relaxation Times for Amorphous IMC:EE Systems Containing 0–100% (w/w) IMC, Measured for Each Component in the Binary Dispersions

IMC:EE Wt%	IMC $T_1$ (s)	EE $T_1$ (s)	IMC $T_{1\rho}$ (ms)	EE $T_{1\rho}$ (ms)
0:100	–	$0.81 \pm 0.02$	–	$17.9 \pm 0.3$
20:80	$1.13 \pm 0.03$	$1.09 \pm 0.01$	$18.6 \pm 0.3$	$19.0 \pm 0.2$
30:70	$1.00 \pm 0.03$	$0.90 \pm 0.01$	$15.5 \pm 0.3$	$15.9 \pm 0.1$
40:60	$1.08 \pm 0.02$	$1.05 \pm 0.02$	$15.9 \pm 0.2$	$16.3 \pm 0.1$
50:50	$1.09 \pm 0.03$	$1.02 \pm 0.01$	$15.2 \pm 0.2$	$15.7 \pm 0.1$
60:40	$1.29 \pm 0.02$	$1.24 \pm 0.01$	$18.2 \pm 0.2$	$17.6 \pm 0.2$
70:30	$1.57 \pm 0.02$	$1.59 \pm 0.05$	$20.5 \pm 0.2$	$19.2 \pm 0.2$
80:20	$2.03 \pm 0.03$	$2.02 \pm 0.08$	$24.3 \pm 0.3$	$23.1 \pm 0.4$
90:10	$2.89 \pm 0.01$	$2.95 \pm 0.08$	$20.5 \pm 0.3$	$17.5 \pm 0.8$
100:0	$3.08 \pm 0.11$	–	$20.2 \pm 0.6$	–

Errors are reported as standard error of the curve fit from 16 data points

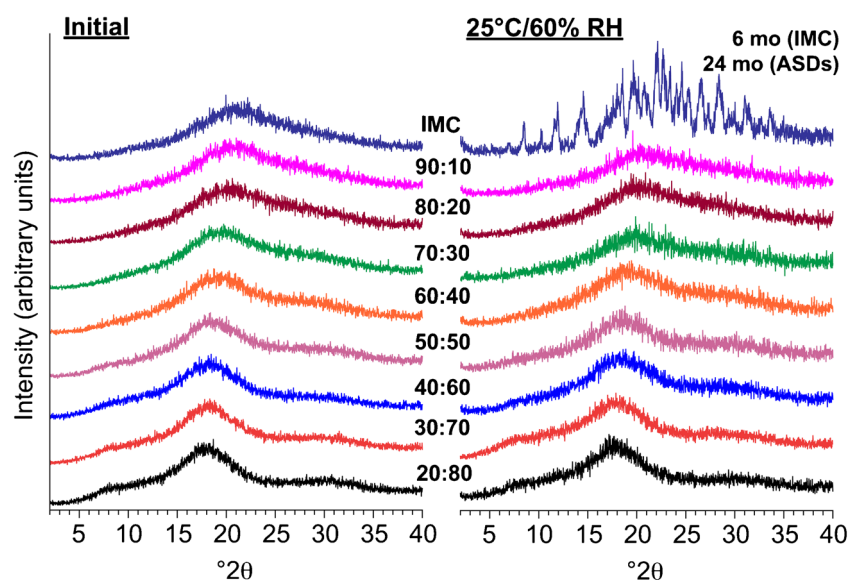
component in a given sample, the two molecules have similar mobility and are likely part of a uniform, single-phase domain.

Figure 6 displays a plot of relaxation times as a function of drug load in ASDs containing 20–90% IMC. The blue (IMC) and red (EE) curves show  $T_1$  values as measured for each individual component in the dispersion at each respective drug load. For example, at 20% IMC, one dataset was acquired using 16 different  $\tau$  saturation recovery delays. Peaks for only IMC were then integrated in the region of 143–124 ppm, peak areas were plotted against  $t$  to give the relaxation curve, and the curve was fit numerically to give the  $T_1$  value for IMC in the ASD. Similarly, peaks areas for only EE were integrated from 49 to 42 ppm and used to calculate  $T_1$  for EE within the ASD. From the plot (Fig. 6) it is evident that the blue (IMC) and red (EE) curves overlay well with each other, indicating that the  $^1\text{H}$

$T_1$  times are similar across the range of drug loads from 20 to 90%. This indicates that the ASD is molecularly dispersed at domain sizes in the range of 65–120 nm ( $L = \sqrt{6DT_1}$ ,  $D \approx 0.8 \text{ nm}^2/\text{ms}$ ) based on the range of absolute  $T_1$  values of 0.9–3.0 s (Table III).

More interesting are the  $^1\text{H}$   $T_{1\rho}$  data, shown in the green (IMC) and purple (EE) curves of Fig. 6. Values were calculated from variable spin-lock datasets in an analogous fashion as for  $T_1$ , with IMC peaks integrated from 143 to 124 ppm and EE peaks integrated from 49 to 42 ppm for 16 different  $^1\text{H}$  spin-lock pulse lengths. From 20 to 60% IMC the green and purple curves overlay well with each other, indicating a uniform molecularly dispersed phase at these drug loads. This phase is assigned to the IMC-EE ionic complex with IMC uniformly distributed throughout the polymeric phase. We know that at 60% IMC there is a small amount of excess free IMC, as all the basic EE side-chains are fully occupied at this drug load. Increasing IMC weight fraction further results in more unbound IMC, which is exactly what was observed in the  $T_{1\rho}$  data. At 70–90% IMC, the green (IMC) and purple (EE) curves diverge from one another, a clear indication of nanoscale phase separation. At these drug loads the data point to two distinct phases: (a) a fully saturated IMC-EE ionic complex, and (b) an IMC-rich phase due to excess IMC. These phases have different mobility and relax at different rates, making the phases detectable in  $^1\text{H}$   $T_{1\rho}$  experiments. At 90% IMC, there are  $7\times$  more IMC carboxyl groups than EE basic groups (Table I), and these IMC groups likely begin to form the H-bonded cyclic dimer that is known for neat amorphous IMC. Based on absolute  $^1\text{H}$   $T_{1\rho}$  values, the IMC-rich domains are on the order of  $\sim 10 \text{ nm}$  ( $L = \sqrt{6DT_1}$ ).

**Fig. 7** PXRD patterns for IMC-EE ASDs ranging from 20 to 90% (w/w) IMC in addition to neat IMC, all prepared by spray drying. The left panel shows samples in their initial state, while the right panel shows the samples after 6 months of storage (neat IMC) or 24 months of storage (ASDs) at 25°C/60% RH. Weight ratios are indicated between the panels.





**Fig. 8** Illustration of the phases present in IMC-EE ASDs as a function of drug load, with associated  $^1\text{H}$  relaxation behavior and EE nitrogen protonation state.

Drug Load	→		
	Low	56%	High
Phase Description	Uniform amorphous IMC:EE ionic complex with free N groups	Uniform amorphous IMC:EE ionic complex	Amorphous IMC:EE ionic complex with excess free IMC
$^1\text{H } T_1$	Same	Same	Same
$^1\text{H } T_{1\rho}$	Same	Same	Different
EE Nitrogen State	Some N Some $\text{NH}^+$	All $\text{NH}^+$	All $\text{NH}^+$
Diagram			

### Powder X-ray Diffraction and Physical Stability

PXRD was used to assess the physical stability of the ASDs upon long term storage. Initial diffraction patterns are shown in the left-hand panel of Fig. 7, and demonstrate that all samples from 20 to 100% (*w/w*) IMC are indeed fully X-ray amorphous after spray drying. Samples were stored at 25°C/60% RH for up to 2 years, and analyzed at 6 and 24 months. After 6 months of storage, neat amorphous IMC has undergone significant crystallization as can be seen in the right-hand panel of Fig. 7. Crystallization from the neat amorphous state appears to be primarily to the metastable  $\alpha$  polymorph. However, even after 2 years of storage all ASDs from 20 to 90% showed no signs of crystallization, indicating exceptional physical stability for even very high drug load dispersions. This shows that only small amounts of polymer may be necessary to stabilize ASDs such as this that take advantage of specific drug-exciipient interactions, regardless of the  $T_g$  and without special storage or packaging requirements. Water content is well known to change as a function of storage time, packaging, and environmental conditions, especially for hygroscopic amorphous formulations. While not the focus of the present study, we expect that water plays a significant role on the phase behavior and drug:excipient interactions in amorphous solid dispersions. This is another large area of pharmaceutical research where solid-state NMR can likely contribute to further our understanding of these complex formulations, and does warrant further study.

### CONCLUSIONS

Ionic bond formation in ASDs has emerged recently as an intriguing formulation option for ionizable yet poorly soluble drug substances. Strong anti-plasticization effects observed using DSC provides a good indication of ionic interactions, and

thus DSC may offer utility as a screening tool to look for these interactions at a small scale. The ionic interaction between indomethacin and Eudragit® E was definitively confirmed in these studies using highly specific  $^{15}\text{N}$  solid-state NMR. In our opinion this method has proven far more selective, specific, and definitive than the more typically applied FTIR. Multinuclear NMR studies are invaluable in studies of formulated materials as it has the power to investigate both drug and excipients simultaneously, as well as interactions among them. Furthermore, this ionic interaction resulted in exquisite physical stability, with no crystallization observed even up to 90% IMC after 2 years of storage.

Using the combined  $^{13}\text{C}$  spectra,  $^{15}\text{N}$  spectra, and  $^1\text{H}$  relaxation data, we determined that at drug loadings of 50% IMC or less the IMC-EE system is a single uniform phase, molecularly dispersed with IMC forming ionic bonds with the EE 2-dimethylaminoethyl side-chains. The nitrogen state of EE shows two populations, its neutral state and a protonated state due to ionic complex formation with IMC. At 60% drug load, the system is primarily a uniform IMC-EE amorphous ionic complex with all EE side-chains ionized and a small amount of excess IMC. At 70–90% IMC there are increasing amounts of free IMC that form drug-rich domains, detectable using  $^1\text{H } T_{1\rho}$  experiments. Figure 8 illustrates the overall phase picture of this system, and we expect this methodology can be applied to any ionically interacting amorphous system.

### REFERENCES

- Hollenbeck RG, Mitrevej KT, Fan AC. Estimation of the extent of drug-exciipient interactions involving croscarmellose sodium. *J Pharm Sci.* 1983;72(3):325–7.
- Ahlneck C, Zograf G. The molecular basis of moisture effects on the physical and chemical stability of drugs in the solid state. *Int J Pharm.* 1990;62(2–3):87–95.

3. Durig T, Fassili AR. Identification of stabilizing and destabilizing effects of excipient-drug interactions in solid dosage form design. *Int J Pharm.* 1993;97(1–3):161–70.
4. Claudius JS, Neau SH. The solution stability of vancomycin in the presence and absence of sodium carboxymethyl starch. *Int J Pharm.* 1998;168(1):41–8.
5. Lu Q, Zografi G. Phase behavior of binary and ternary amorphous mixtures containing indomethacin, citric acid, and PVP. *Pharm Res.* 1998;15(8):1202–6.
6. Byrn SR, Xu W, Newman AW. Chemical reactivity in solid-state pharmaceuticals: formulation implications. *Adv Drug Deliv Rev.* 2001;48(1):115–36.
7. McDaid FM, Barker SA, Fitzpatrick S, Petts CR, Craig DQM. Further investigations into the use of high sensitivity differential scanning calorimetry as a means of predicting drug-excipient interactions. *Int J Pharm.* 2003;252(1–2):235–40.
8. Bandi N, Wei W, Roberts CB, Kotra LP, Kompella UB. Preparation of budesonide- and indomethacin-hydroxypropyl- $\beta$ -cyclodextrin (HPBCD) complexes using a single-step, organic-solvent-free supercritical fluid process. *Eur J Pharm Sci.* 2004;23(2):159–68.
9. Vueba M, Veiga F, Sousa J, Pina ME. Compatibility studies between ibuprofen or ketoprofen with cellulose ether polymer mixtures using thermal analysis. *Drug Dev Ind Pharm.* 2005;31(10):943–9.
10. Batista de Carvalho LAE, Marques MPM, Tomkinson J. Drug-excipient interactions in ketoprofen: a vibrational spectroscopy study. *Biopolymers.* 2006;82(4):420–4.
11. Balani PN, Wong SY, Ng WK, Widjaja E, Tan RBH, Chan SY. Influence of polymer content on stabilizing milled amorphous salbutamol sulphate. *Int J Pharm.* 2010;391(1–2):125–36.
12. Bharate SS, Bharate SB, Bajaj AN. Interactions and incompatibilities of pharmaceutical excipients with active pharmaceutical ingredients: a comprehensive review. *J Excipients Food Chem.* 2010;1(3):3–26.
13. Sperger DM. Solid-state NMR analysis of excipients and drug-excipient interactions in the amorphous state. PhD Thesis; 2010. 259 pp.
14. Narang AS, Desai D, Badawy S. Impact of excipient interactions on solid dosage form stability. *Pharm Res.* 2012;29(10):2660–83.
15. Panakanti R, Narang AS. Impact of excipient interactions on drug bioavailability from solid dosage forms. *Pharm Res.* 2012;29(10):2639–59.
16. Dordevic SM, Radulovic TS, Cekic ND, Randelovic DV, Savic MM, Krajcisinik DR, *et al.* Experimental design in formulation of diazepam nanoemulsions: physicochemical and pharmacokinetic performances. *J Pharm Sci.* 2013;102(11):4159–72.
17. Chadha R, Bhandari S. Drug-excipient compatibility screening-role of thermoanalytical and spectroscopic techniques. *J Pharm Biomed Anal.* 2014;87:82–97.
18. Sachin TV, Deodhar MN, Prakya V. Advances in analytical techniques used in predicting drug-excipient interactions. *Int J Pharm Technol.* 2014;6(1):6388–417. 6330 pp
19. Tita B, Ledeti I, Bandur G, Tita D. Compatibility study between indomethacin and excipients in their physical mixtures. *J Therm Anal Calorim.* 2014;118(2):1293–304.
20. Chakravarty P, Kothari S, Deese A, Lubach JW. Solid-state characterization of novel propylene glycol ester solvates isolated from lipid formulations. *Mol Pharm.* 2015;12(7):2551–7.
21. Schou-Pedersen AMV, Oestergaard J, Cornett C, Hansen SH. Evaluation of microwave oven heating for prediction of drug-excipient compatibilities and accelerated stability studies. *Int J Pharm.* 2015;485(1–2):97–107.
22. Lubach JW, Padden BE, Winslow SL, Salsbury JS, Masters DB, Topp EM, *et al.* Solid-state NMR studies of pharmaceutical solids in polymer matrices. *Anal Bioanal Chem.* 2004;378(6):1504–10.
23. Ueda H, Aikawa S, Kashima Y, Kikuchi J, Ida Y, Tanino T, *et al.* Anti-plasticizing effect of amorphous indomethacin induced by specific intermolecular interactions with PVA copolymer. *J Pharm Sci.* 2014;103(9):2829–38.
24. Yuan X, Xiang T-X, Anderson BD, Munson EJ. Hydrogen bonding interactions in amorphous indomethacin and its amorphous solid dispersions with poly(vinylpyrrolidone) and poly(vinylpyrrolidone-co-vinyl acetate) studied using  $^{13}\text{C}$  solid-state NMR. *Mol Pharm.* 2015;12(12):4518–28.
25. Taylor LS, Zografi G. Spectroscopic characterization of interactions between PVP and indomethacin in amorphous molecular dispersions. *Pharm Res.* 1997;14(12):1691–8.
26. Watanabe T, Ohno I, Wakiyama N, Kusai A, Senna M. Stabilization of amorphous indomethacin by co-grinding in a ternary mixture. *Int J Pharm.* 2002;241(1):103–11.
27. Takeuchi H, Nagira S, Yamamoto H, Kawashima Y. Solid dispersion particles of amorphous indomethacin with fine porous silica particles by using spray-drying method. *Int J Pharm.* 2005;293(1–2):155–64.
28. Vyazovkin S, Dranca I. Effect of physical aging on nucleation of amorphous indomethacin. *J Phys Chem B.* 2007;111(25):7283–7.
29. Bhugra C, Shmeis R, Pikal MJ. Role of mechanical stress in crystallization and relaxation behavior of amorphous indomethacin. *J Pharm Sci.* 2008;97(10):4446–58.
30. Alonzo DE, Zhang GGZ, Zhou D, Gao Y, Taylor LS. Understanding the behavior of amorphous pharmaceutical systems during dissolution. *Pharm Res.* 2010;27(4):608–18.
31. Greco K, Bogner R. Crystallization of amorphous indomethacin during dissolution: effect of processing and annealing. *Mol Pharm.* 2010;7(5):1406–18.
32. Karmwar P, Boetker JP, Graeser KA, Strachan CJ, Rantanen J, Rades T. Investigations on the effect of different cooling rates on the stability of amorphous indomethacin. *Eur J Pharm Sci.* 2011;44(3):341–50.
33. Ayenew Z, Paudel A, Rombaut P, Van den Mooter G. Effect of compression on non-isothermal crystallization behaviour of amorphous indomethacin. *Pharm Res.* 2012;29(9):2489–98.
34. Xiang T-X, Anderson BD. Molecular dynamics simulation of amorphous indomethacin. *Mol Pharm.* 2013;10(1):102–14.
35. Lin S-Y, Lin H-L, Chi Y-T, Huang Y-T, Kao C-Y, Hsieh W-H. Thermoanalytical and fourier transform infrared spectral curve-fitting techniques used to investigate the amorphous indomethacin formation and its physical stability in Indomethacin-Soluplus solid dispersions. *Int J Pharm.* 2015;496(2):457–65.
36. Thakral NK, Mohapatra S, Stephenson GA, Suryanarayanan R. Compression-induced crystallization of amorphous indomethacin in tablets: characterization of spatial heterogeneity by two-dimensional x-ray diffractometry. *Mol Pharm.* 2015;12(1):253–63.
37. Hattori Y, Otsuka M. Analysis of the stabilization process of indomethacin crystals via  $\pi$ - $\pi$  and CH- $\pi$  interactions measured by Raman spectroscopy and X-ray diffraction. *Chem Phys Lett.* 2016;661:114–8.
38. Chokshi RJ, Shah NH, Sandhu HK, Malick AW, Zia H. Stabilization of low glass transition temperature indomethacin formulations: impact of polymer-type and its concentration. *J Pharm Sci.* 2008;97(6):2286–98.
39. Sarode AL, Sandhu H, Shah N, Malick W, Zia H. Hot melt extrusion for amorphous solid dispersions: temperature and moisture activated drug-polymer interactions for enhanced stability. *Mol Pharm.* 2013;10(10):3665–75.
40. Kojima T, Higashi K, Suzuki T, Tomono K, Moribe K, Yamamoto K. Stabilization of a supersaturated solution of mefenamic acid from a solid dispersion with EUDRAGIT EPO. *Pharm Res.* 2012;29(10):2777–91.

41. Liu H, Zhang X, Suwardie H, Wang P, Gogos CG. Miscibility studies of indomethacin and Eudragit E PO by thermal, rheological, and spectroscopic analysis. *J Pharm Sci*. 2012;101(6):2204–12.
42. Weuts I, Kempen D, Verreck G, Peeters J, Brewster M, Bleton N, *et al*. Salt formation in solid dispersions consisting of polyacrylic acid as a carrier and three basic model compounds resulting in very high glass transition temperatures and constant dissolution properties upon storage. *Eur J Pharm Sci*. 2005;25(4–5):387–93.
43. Song Y, Yang X, Chen X, Nie H, Byrn S, Lubach JW. Investigation of drug-excipient interactions in lapatinib amorphous solid dispersions using solid-state NMR spectroscopy. *Mol Pharm*. 2015;12(3):857–66.
44. Song Y, Zemlyanov D, Chen X, Nie H, Su Z, Fang K, *et al*. Acid-base interactions of polystyrene sulfonic acid in amorphous solid dispersions using a combined UV/FTIR/XPS/ssNMR study. *Mol Pharm*. 2016;13(2):483–92.
45. Song Y, Zemlyanov D, Chen X, Su Z, Nie H, Lubach JW, *et al*. Acid-base interactions in amorphous solid dispersions of lumefantrine prepared by spray-drying and hot-melt extrusion using X-ray photoelectron spectroscopy. *Int J Pharm*. 2016;514(2):456–64.
46. Metz G, Wu X, Smith SO. Ramped-amplitude cross polarization in magic-angle-spinning NMR. *J Magn Reson Ser A*. 1994;110(2):219–27.
47. Pines A, Gibby MG, Waugh JS. Proton-enhanced nuclear induction spectroscopy. Method for high-resolution NMR of dilute spins in solids. *J Chem Phys*. 1972;56(4):1776–7.
48. Stejskal EO, Schaefer J, Waugh JS. Magic-angle spinning and polarization transfer in proton-enhanced NMR. *J Magn Reson* (1969–1992). 1977;28(1):105–12.
49. Dixon WT, Schaefer J, Sefcik MD, Stejskal EO, McKay RA. Total suppression of sidebands in CPMAS carbon-13 NMR. *J Magn Reson* (1969–1992). 1982;49(2):341–5.
50. Song Z, Antzutkin ON, Feng X, Levitt MH. Sideband suppression in magic-angle-spinning NMR by a sequence of 5 pi pulses. *Solid State Nucl Magn Reson*. 1993;2(3):143–6.
51. Fung BM, Khitrin AK, Ermolaev K. An improved broadband decoupling sequence for liquid crystals and solids. *J Magn Reson*. 2000;142(1):97–101.
52. Barich DH, Gorman EM, Zell MT, Munson EJ. 3-Methylglutaric acid as a  $^{13}\text{C}$  solid-state NMR standard. *Solid State Nucl Magn Reson*. 2006;30(3–4):125–9.
53. Hayashi S, Hayamizu K. Chemical shift standards in high-resolution solid-state NMR. 2. Nitrogen-15 nuclei. *Bull Chem Soc Jpn*. 1991;64(2):688–90.
54. Hancock BC, Shamblin SL, Zografi G. Molecular mobility of amorphous pharmaceutical solids below their glass transition temperatures. *Pharm Res*. 1995;12(6):799–806.
55. Couchman PR. Composition-dependent glass-transition temperatures and copolymers. *Nature*. 1982;298(5876):729–30.
56. Couchman PR, Karasz FE. A classical thermodynamic discussion of the effect of composition on glass-transition temperatures. *Macromolecules*. 1978;11(1):117–9.
57. Chiang P-C, Cui Y, Ran Y, Lubach J, Chou K-J, Bao L, *et al*. In vitro and in vivo evaluation of amorphous solid dispersions generated by different bench-scale processes, using griseofulvin as a model compound. *AAPS J*. 2013;15(2):608–17.
58. Yuan X, Sperger D, Munson EJ. Investigating miscibility and molecular mobility of nifedipine-PVP amorphous solid dispersions using solid-state NMR spectroscopy. *Mol Pharm*. 2014;11(1):329–37.
59. Pham TN, Watson SA, Edwards AJ, Chavda M, Clawson JS, Strohmeier M, *et al*. Analysis of amorphous solid dispersions using 2D solid-state NMR and  $^1\text{H}$   $T_1$  relaxation measurements. *Mol Pharm*. 2010;7(5):1667–91.
60. Chakravarty P, Lubach JW, Hau J, Nagapudi K. A rational approach towards development of amorphous solid dispersions: experimental and computational techniques. *Int J Pharm*. 2017;519(1–2):44–57.